

CHIRAL DYNAMICS AND NUCLEAR MATTER¹

N. Kaiser ^a, S. Fritsch ^a and W. Weise ^{a,b}

^a Physik Department, Technische Universität München, D-85747 Garching, Germany

^b ECT*, I-38050 Villazzano (Trento), Italy

email: nkaiser@physik.tu-muenchen.de

Abstract

We calculate the equation of state of isospin-symmetric nuclear matter in the three-loop approximation of chiral perturbation theory. The contributions to the energy per particle $\bar{E}(k_f)$ from one- and two-pion exchange diagrams are ordered in powers of the Fermi momentum k_f (modulo functions of k_f/m_π). It is demonstrated that, already at order $\mathcal{O}(k_f^4)$, two-pion exchange produces realistic nuclear binding. The underlying saturation mechanism is surprisingly simple (in the chiral limit), namely the combination of an attractive k_f^3 -term and a repulsive k_f^4 -term. The empirical saturation point and the nuclear compressibility $K \simeq 250$ MeV are well reproduced at order $\mathcal{O}(k_f^5)$ with a momentum cut-off of $\Lambda \simeq 0.65$ GeV which parametrizes short-range dynamics. No further short-distance terms are required in our calculation of nuclear matter. In the same framework we calculate the density-dependent asymmetry energy and find $A_0 \simeq 34$ MeV at the saturation point, in good agreement with the empirical value. The pure neutron matter equation of state is also in fair qualitative agreement with sophisticated many-body calculations and a resummation result of effective field theory, but only for low neutron densities $\rho_n < 0.25$ fm⁻³.

PACS: 12.38.Bx, 21.65.+f

Keywords: Effective field theory at finite density; Nuclear matter equation of state; Asymmetry energy, Neutron matter.

1 Introduction

One of the basic problems in nuclear physics has traditionally been to develop a microscopic understanding of the nuclear matter equation of state and the properties of finite nuclei in terms of the underlying free nucleon-nucleon interaction. The present status is that a quantitatively successful description of nuclear matter can be achieved, using advanced many-body techniques, in a non-relativistic framework when invoking an adjustable three-body force [1]. Alternative relativistic approaches treat nucleons as Dirac-particles. The simplest one in this category is the $\sigma\omega$ -mean field model of Serot and Walecka [2]. It describes nucleons as Dirac-quasiparticles moving in self-consistently generated scalar and vector mean fields. With two couplings adjusted to the empirical saturation point, the nuclear compressibility comes out however much too large

¹Work supported in part by BMBF, GSI and DFG.

(by a factor of 2). Refinements of relativistic mean field models which include additional non-linear terms with adjustable parameters, are nowadays widely used for the calculation of nuclear matter properties and finite nuclei [3]. The more basic Dirac-Brückner approach of Brockmann and Machleidt [4] solves a relativistically improved Bethe-Goldstone equation with a realistic nucleon-nucleon interaction parametrized in terms of one-boson exchange potentials.

During the last decade, a novel approach to the NN-interaction based on effective field theory (in particular chiral perturbation theory) has emerged [5, 6, 7, 8]. The key element is a power counting scheme which relies on the separation of long and short distance dynamics. The methods of effective field theory have recently been applied to systems at finite density in refs.[9, 10]. These works deal mainly with the effective range expansion (and generalizations thereof) of the equation of state of a dilute many-fermion system. The complete resummation of in-medium multi-loop diagrams for a system with an unnaturally large scattering length (such as neutron matter) has been achieved in ref.[11] (in the limit of infinite space-time dimensions). Lutz et al. [12] have calculated the equation of state of nuclear matter from chiral pion-nucleon dynamics. The contributions of one- and two-pion exchange diagrams to the energy per particle have been evaluated up to fourth order in small momenta. An essential ingredient in their work is an additionally introduced attractive zero-range NN-contact interaction. The saturation point obtained in this calculation depends very sensitively on the numerical value of $g_A^2/2 + g_0 + g_1$, the strength of this NN-contact interaction. The dynamical origin of the important attractive NN-contact interaction remains unexplained. Furthermore, the two components of the contact interaction, the one proportional to $g_A^2/2$ and the other one parametrized by a coupling $g_0 + g_1$, have not been treated on equal footing in ref.[12] when going to higher orders in perturbation theory.

In its starting point our approach to the nuclear matter problem is closely related to the work of ref.[12]. We also use the three-loop approximation of chiral perturbation theory at finite density to calculate the contributions of one- and two-pion exchange diagrams to the energy per particle of isospin symmetric nuclear matter. In a systematic non-relativistic expansion we compute all terms up-to-and-including fifth order in small momenta (these are the Fermi momentum k_f and the pion mass m_π) and thus go one order beyond the work of ref.[12]. A major difference in comparison with ref.[12] is that we do not introduce any zero-range NN-contact interactions with adjustable strengths in addition to the chiral pion-exchange terms. Instead we use a momentum-space cut-off Λ to regularize the few divergent parts associated with the chiral two-pion exchange, and we keep the power divergences which are specific for cut-off regularization. Their contribution to the energy per particle is equivalent to that of a zero-range contact interaction parametrized through the scale Λ , which then represents the short-distance dynamics. This relationship is very useful in order to understand the saturation mechanism underlying the chiral two-pion exchange, as we shall discuss. A further feature of our treatment is that the properties of isospin symmetric nuclear matter (saturation point and compressibility) and of isospin asymmetric nuclear matter (asymmetry energy and equation of state of pure neutron matter) are given in terms of only *one* adjustable parameter, namely the cut-off Λ . It is then highly non-trivial to satisfy all known empirical constraints by fine-tuning just this one single scale Λ to a physically sensible value. We demonstrate that this is indeed possible. The present chiral perturbation theory calculation allows to systematically explore the role that chiral symmetry plays in the nuclear matter problem.

Our paper is organized as follows. In section 2 we perform the chiral (or small momentum) expansion of the nuclear matter equation of state up-to-and-including terms of order $\mathcal{O}(k_f^5)$. We present analytical results for the energy per particle $\bar{E}(k_f)$ as given by 1π -exchange, iterated 1π -exchange and irreducible 2π -exchange diagrams. Then we discuss the saturation mechanism and the properties of our nuclear matter equation of state. In section 3 we calculate the density dependent asymmetry energy $A(k_f)$ in the same framework and discuss the corresponding results.

Section 4 is devoted to the equation of state of pure neutron matter as it follows from the same set of pion-exchange diagrams. Finally, section 5 ends with a summary and an outlook.

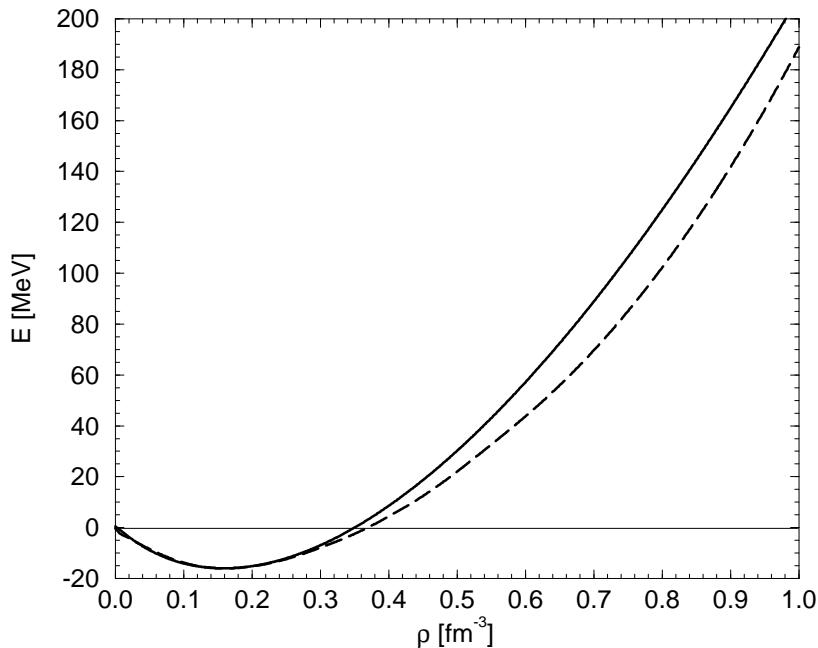


Fig. 1: Equation of state of isospin symmetric nuclear matter. The full line gives the parametrization eq.(1) with $\alpha = 5.27$ and $\beta = 12.22$. The dashed line stems from the many-body calculation of ref.[15].

Before presenting results of our (perturbative) diagrammatic calculation we like to draw attention to the following fact. A simple but nevertheless realistic parametrization of the energy per particle of isospin symmetric nuclear matter is given by the following expression,

$$\bar{E}(k_f) = \frac{3k_f^2}{10M} - \alpha \frac{k_f^3}{M^2} + \beta \frac{k_f^4}{M^3}, \quad (1)$$

with k_f the Fermi momentum related to the nucleon density in the usual way, $\rho = 2k_f^3/3\pi^2$, and $M = 939$ MeV the (free) nucleon mass. The first term in eq.(1) is the well-known kinetic energy contribution of a Fermi gas and the powers of M in the other terms have been chosen such that α and β are dimensionless. The two-parameter form eq.(1) has generically a saturation minimum if $\alpha, \beta > 0$. The interesting feature of this parametrization is that once α and β are adjusted to the empirical nuclear matter saturation point, $k_{f0} = (1.35 \pm 0.05) \text{ fm}^{-1}$ and $\bar{E}_0 = \bar{E}(k_{f0})$, the nuclear matter compressibility [13, 14],

$$K = k_{f0}^2 \left. \frac{\partial^2 \bar{E}(k_f)}{\partial k_f^2} \right|_{k_f=k_{f0}} = (250 \pm 25) \text{ MeV}, \quad (2)$$

comes out correctly. For example, adjusting to the saturation point obtained in the sophisticated many-body calculation of the Urbana group [15], $\rho_0 = 2k_{f0}^3/3\pi^2 = 0.159 \text{ fm}^{-3}$ and $\bar{E}_0 = -16.0$ MeV, one finds $\alpha = 5.27$ and $\beta = 12.22$, and the compressibility is *predicted* as $K = 236$ MeV. In Fig. 1 we compare the density dependence of $\bar{E}(k_f)$, given by eq.(1) (full line) with the equation of state resulting from the many-body calculation of ref.[15] (dashed line). One

observes that the relative deviations of both curves do not exceed 10% up to quite high densities, $\rho = 1.0 \text{ fm}^{-3}$. Keeping in mind that eq.(1) provides a realistic parametrization of the nuclear matter equation of state will be very useful in order to understand the saturation mechanism underlying the chiral two-pion exchange. In the chiral limit ($m_\pi = 0$) and truncating to order $\mathcal{O}(k_f^4)$, the equation of state following from one- and two-pion exchange will be precisely of the form, eq.(1).

2 Chiral expansion of the nuclear matter equation of state

The tool in order to systematically investigate the consequences of spontaneous and explicit chiral symmetry breaking in QCD is chiral perturbation theory. Observables are calculated with the help of an effective field theory formulated in terms of the Goldstone bosons (pions) and the low-lying baryons (nucleons). The diagrammatic expansion in the number of loops has a one-to-one correspondence to a systematic expansion of observables in small external momenta and meson (or quark) masses. For the problem under consideration, the external momentum is the Fermi momentum k_f , related to the nucleon density $\rho = 2k_f^3/3\pi^2$. The relevant observable is the energy per particle $\bar{E}(k_f)$, i.e. the ratio of energy density and particle density, with the free nucleon mass M subtracted. Consequently, the equation of state of nuclear matter as given by chiral perturbation theory will be of the form of an expansion in powers of the Fermi momentum k_f . The expansion coefficients are however non-trivial functions of k_f/m_π , the dimensionless ratio of the two relevant small scales inherent to the problem. Note that at the empirical saturation point, $k_{f0} \simeq 2m_\pi$, so that both scales are of comparable magnitude for the densities of interest. This also implies that pions have to be kept as explicit degrees of freedom. At the saturation density pionic effects cannot be properly accounted for just by coefficients of local NN-contact interactions which form the basis of effective range expansions at finite density [10].

Naive chiral power counting (which is basically a counting in terms of mass dimension) suggests that closed vacuum diagrams with L loops (which represent the ground state energy density in diagrammatic language) give rise to a contribution to the energy per particle of the form $\bar{E}(k_f) = k_f^{2L-1} \mathcal{F}_L(k_f/m_\pi)$. However, the two-nucleon system is known to provide exceptions to the naive counting rules by the so-called iterated one-pion exchange. In that case the relevant energy denominator is a difference of nucleon kinetic energies, and this implies that the large scale factor M (the nucleon mass) appears in the numerator of the Feynman amplitude [7]. There are indeed certain closed three-loop diagrams (see Fig. 3) which contribute to the energy per particle already at order $\mathcal{O}(k_f^4)$ [12]. By the same argument one expects that the four-loop Fock-diagram² which includes the twice-iterated one-pion exchange (proportional to M^2) will contribute already at order $\mathcal{O}(k_f^5)$. Luckily, the analogous four-loop Hartree-diagram³ vanishes when taking the spin- or Dirac-trace. Because of the enormous complexity of four-loop diagrams we restrict ourselves to the computation of all contributions up-to-and-including order $\mathcal{O}(k_f^5)$ as they are given by closed three-loop diagrams.

The only new ingredient in performing calculations at finite nucleon density (as compared to calculations of scattering processes in the vacuum) is the in-medium nucleon propagator. It expresses the fact that the ground-state of the system has changed from an empty vacuum to a filled Fermi sea of nucleons. In its relativistic form this in-medium propagator of a nucleon with

²Obtained by drawing in the right diagram in Fig. 3, a third pion-line intersecting both the other two.

³Obtained by drawing in the left diagram in Fig. 3 a third parallel pion-line connecting both equally oriented nucleon rings.

four-momentum $p^\mu = (p_0, \vec{p})$ reads

$$(\not{p} + M) \left\{ \frac{i}{p^2 - M^2 + i\epsilon} - 2\pi \delta(p^2 - M^2) \theta(p_0) \theta(k_f - |\vec{p}|) \right\}. \quad (3)$$

Note that eq.(3) splits additively into the vacuum nucleon propagator and a medium insertion (i.e. the piece involving an on-shell delta-function and step-functions). This allows to organize the diagrammatic calculation according to the number of medium insertions. Diagrams with no medium insertion lead to an unobservable shift of the vacuum energy. Diagrams with exactly one medium insertion just renormalize the nucleon mass to its measured value M (because of the presence of one single on-shell delta-function). The really interesting many-body effects from interactions start thus with diagrams having two or more medium insertions.

The pion-nucleon interaction vertices relevant in this work are the pseudovector πNN -vertex and the Tomozawa-Weinberg $\pi\pi NN$ -contact vertex of the form,

$$\frac{g_A}{2f_\pi} \not{q}_a \gamma_5 \tau_a, \quad \frac{1}{4f_\pi^2} (\not{q}_b - \not{q}_a) \epsilon_{abc} \tau_c. \quad (4)$$

Here, the pion four-momenta $q_{a,b}$ are out-going ones and $f_\pi = 92.4 \text{ MeV}$ denotes the weak pion decay constant. For the nucleon axial vector coupling constant g_A we choose the value $g_A = 1.3$. Via the Goldberger-Treiman relation this corresponds to a πNN -coupling constant of $g_{\pi N} = g_A M / f_\pi = 13.2$ which agrees with present empirical determinations of $g_{\pi N}$ from πN -dispersion relation analyses [16].

2.1 Kinetic energy

The first contribution to the energy per particle $\bar{E}(k_f)$ is the kinetic energy of a non-interacting relativistic Fermi gas of nucleons. Expanding $\sqrt{M^2 + \vec{p}^2} - M$ in powers of $1/M$ and integrating over a Fermi sphere of radius k_f one gets,

$$\bar{E}_k(k_f) = \frac{3k_f^2}{10M} - \frac{3k_f^4}{56M^3}. \quad (5)$$

For the densities $\rho = 2k_f^3/3\pi^2$ of interest this series converges very rapidly. The next term in this series, $k_f^6/48M^5$, is already negligibly small.

2.2 One-pion exchange

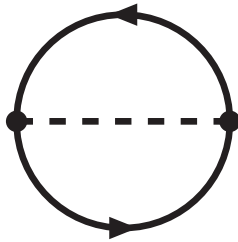


Fig.2: The one-pion exchange Fock-diagram. Solid and dashed lines represent nucleons and pions, respectively. The combinatoric factor of this diagram is $1/2$.

The one-pion exchange Hartree-diagram is trivially zero (since $q^\mu = 0$) and the one-pion exchange Fock-diagram is shown in Fig.2. The interesting many-body effect comes from the

medium insertion at each nucleon propagator. In that case the two loop-integrations convert into integrals over Fermi spheres of radius k_f . After taking the Dirac-trace of the product of $(\not{p} + M)$ -factors and pseudovector πN -interaction vertices one performs a (non-relativistic) $1/M$ -expansion of the complete integrand. In this form all integrals can be solved analytically and the result for the 1π -exchange Fock-diagram reads,

$$\begin{aligned} \bar{E}_1(k_f) = & \frac{3g_A^2 m_\pi^3}{(4\pi f_\pi)^2} \left\{ \frac{u^3}{3} + \frac{1}{8u} - \frac{3u}{4} + \arctan 2u - \left(\frac{3}{8u} + \frac{1}{32u^3} \right) \ln(1 + 4u^2) \right. \\ & \left. + \frac{m_\pi^2}{40M^2} \left[\frac{40}{3}u^3 - 8u^5 + 9u + \frac{1}{2u} - (12u^2 + 5) \arctan 2u - \frac{1}{8u^3} \ln(1 + 4u^2) \right] \right\}, \quad (6) \end{aligned}$$

Here, we have introduced the abbreviation $u = k_f/m_\pi$. The terms proportional to u^3 and $u^5 m_\pi^2/M^2$ in eq.(6) correspond to the (repulsive) zero-range contact interaction produced by any pseudoscalar meson exchange. The $1/M$ -expansion is again converging rapidly. For example, at $k_f = 270$ MeV the $1/M^2$ -correction (second line in eq.(6)) is only -5.2% of the leading order term (first line in eq.(6)). Note also, the Taylor-series expansion of $\bar{E}_1(k_f)$ in eq.(6) converges only for $k_f \leq m_\pi/2$. This would correspond to tiny densities of $\rho \leq 0.0027$ fm $^{-3}$.

2.3 Iterated one-pion exchange

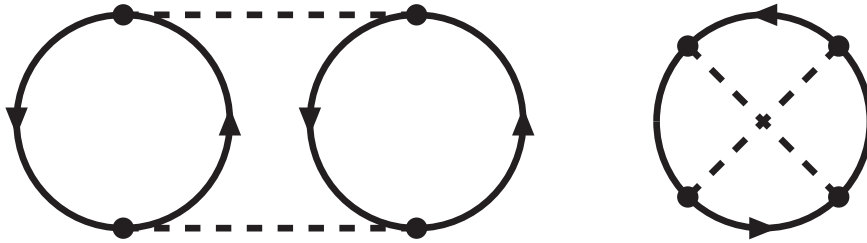


Fig.3: Iterated one-pion exchange Hartree and Fock-diagrams. The combinatoric factor of these diagrams is $1/4$.

Next, we consider the three-loop diagrams shown in Fig. 3. With two medium insertions on neighboring nucleon propagators they contribute, via mass and coupling constant renormalization, to the one-pion exchange Fock-diagram. These effects are automatically taken care of in eq.(6) by using the physical input parameters. Considering two medium insertions on non-neighboring nucleon propagators we encounter the planar box graph [7]. In a non-relativistic $1/M$ -expansion the first contribution from the planar box graph is the iterated 1π -exchange which is enhanced by the large scale factor M . In case of the left diagram in Fig. 3 (Hartree-diagram) the inner loop integral becomes equal to the iterated 1π -exchange amplitude in forward direction. Using the analytical results given in section 4.3 of ref.[7], we can even perform the remaining integral over the two Fermi spheres of radius k_f . Altogether, we find for the Hartree-diagram in Fig. 3 with two medium insertions,

$$\bar{E}_2(k_f) = \frac{3g_A^4 M m_\pi^4}{5(8\pi)^3 f_\pi^4} \left\{ \frac{9}{2u} - 59u + (60 + 32u^2) \arctan 2u - \left(\frac{9}{8u^3} + \frac{35}{2u} \right) \ln(1 + 4u^2) \right\}. \quad (7)$$

Note that this expression does not include the contribution of a linear divergence $\int_0^\infty dl$ of the momentum space loop integral occurring in the Hartree-diagram. In dimensional regularization such a linear divergence is set to zero, whereas in cut-off regularization it equals

the momentum space cut-off Λ . There is an interpretational problem with the result eq.(7) when using dimensional regularization. While eq.(7) alone gives sizeable repulsion, for example $\bar{E}_2(k_f = 270 \text{ MeV}) = 50.0 \text{ MeV}$, second order perturbation theory arguments suggest attraction (because the intermediate-states lie mostly higher in energy than the initial or final state). The source of this apparent contradiction is the linear divergence $\int_0^\infty dl 1$. Using cut-off regularization together with a large enough value of Λ one regains the expected attraction. The additional additive terms specific for cut-off regularization are collected in eq.(15). The evaluation of the right diagram in Fig. 3 (Fock-diagram) with two medium insertions is very similar. There one encounters the iterated 1π -exchange amplitude in backward direction [7]. Putting all pieces together one obtains the following result for the Fock-diagram in Fig. 3 with two medium insertions,

$$\bar{E}_3(k_f) = \frac{g_A^4 M m_\pi^4}{(4\pi)^3 f_\pi^4} \left\{ \frac{u^3}{2} + \int_0^u dx \frac{3x(u-x)^2(2u+x)}{2u^3(1+2x^2)} [(1+8x^2+8x^4) \arctan x - (1+4x^2) \arctan 2x] \right\}, \quad (8)$$

where we have again transferred the linear divergence proportional to the cut-off Λ to eq.(15).

Next, we consider the diagrams in Fig. 3 with three medium insertions. In this case one has to evaluate an integral over the product of three Fermi spheres of radius k_f . Suitable techniques allow to perform most of these nine integrations analytically. For the Hartree-diagram in Fig. 3 with three medium insertions we end up with the following representation,

$$\bar{E}_4(k_f) = \frac{9g_A^4 M m_\pi^4}{(4\pi f_\pi)^4 u^3} \int_0^u dx x^2 \int_{-1}^1 dy [2uxy + (u^2 - x^2 y^2) H] \left\{ \frac{2s^2 + s^4}{1 + s^2} - 2 \ln(1 + s^2) \right\}, \quad (9)$$

$$H = \ln \frac{u + xy}{u - xy}, \quad s = xy + \sqrt{u^2 - x^2 + x^2 y^2}. \quad (10)$$

Similarly, we find for the Fock-diagram in Fig. 3 with three medium insertions the representation,

$$\bar{E}_5(k_f) = \frac{9g_A^4 M m_\pi^4}{(4\pi f_\pi)^4 u^3} \int_0^u dx \left\{ \frac{G^2}{8} + \frac{x^2}{4} \int_{-1}^1 dy \int_{-1}^1 dz \frac{yz \theta(y^2 + z^2 - 1)}{|yz| \sqrt{y^2 + z^2 - 1}} [s^2 - \ln(1 + s^2)] [\ln(1 + t^2) - t^2] \right\}, \quad (11)$$

with the auxiliary functions,

$$G = u(1 + u^2 + x^2) - \frac{1}{4x} [1 + (u + x)^2][1 + (u - x)^2] \ln \frac{1 + (u + x)^2}{1 + (u - x)^2}, \quad (12)$$

$$t = xz + \sqrt{u^2 - x^2 + x^2 z^2}. \quad (13)$$

For the numerical evaluation of the $dydz$ -double integral in eq.(11) it is advantageous to first antisymmetrize the integrand both in y and z and then to substitute $z = \sqrt{y^2 \zeta^2 + 1 - y^2}$. This way the integration region becomes equal to the unit-square $0 \leq y, \zeta \leq 1$. We note that our results, eqs.(7,8,9,11), which comprise all 2π -exchange contributions at order $\mathcal{O}(k_f^4)$, agree with those of ref.[12] after suitable simplification. As a further check on the whole formalism we rederived the analytical result of Onsager et al. [17] for the two-photon exchange Fock-diagram of the electron-gas, $\bar{E} = [(\ln 2/3) - (3\zeta(3)/2\pi^2)] Rydberg$, using the same techniques.

The diagrams in Fig. 3 with four medium insertions do not have to be calculated explicitly. These are purely imaginary and they are cancelled by the imaginary parts coming along with the diagrams with two and three medium insertions. Via unitarity, such imaginary parts are related to on-shell scattering of nucleons. Energy conservation and Pauli-blocking in the medium leave no phase-space for these processes and thus the energy per particle $\bar{E}(k_f)$ remains a real quantity (as it must of course be).

2.4 Irreducible two-pion exchange

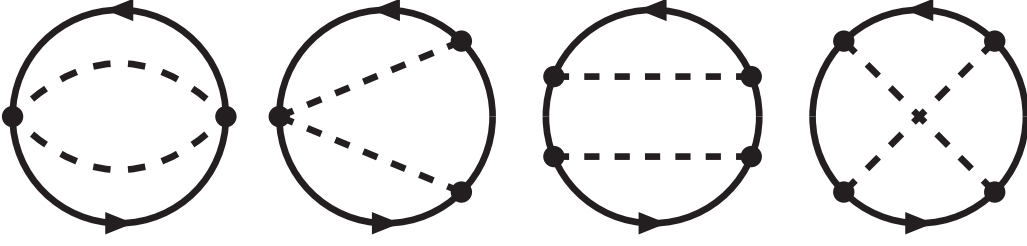


Fig.4: Irreducible two-pion exchange Fock-diagrams. The corresponding Hartree-diagrams vanish for isospin symmetric nuclear matter. The combinatoric factors of these diagrams are $1/4$, 1 , $1/2$ and $1/4$, in the order shown.

Contributions of three-loop 2π -exchange diagrams to $\bar{E}(k_f)$ at order $\mathcal{O}(k_f^5)$ are in accordance with the naive chiral power counting rules. The relevant 2π -exchange Fock-diagrams are shown in Fig. 4. Considering two medium insertions at the upper and lower nucleon propagators one finds that their contribution to the energy per particle can be expressed in terms of the T-matrix related to the irreducible 2π -exchange. This T-matrix has been evaluated in section 4.2 of ref.[7] using dimensional regularization. The result of cut-off regularization differs only little by some coefficients of purely polynomial terms and the presence of a quadratic divergence Λ^2 (see also appendix A in ref.[6]). After performing the remaining integral over two Fermi spheres of radius k_f one ends up with the following analytical expression for the Fock-diagrams in Fig. 4,

$$\begin{aligned}
\bar{E}_6(k_f) = & \frac{m_\pi^5}{(4\pi f_\pi)^4} \left\{ \left[\frac{3}{32u^3}(43g_A^4 + 6g_A^2 - 1) + \frac{3}{4u}(23g_A^4 + 2g_A^2 - 1) \right] \ln^2(u + \sqrt{1+u^2}) \right. \\
& + \left[\frac{u^4}{5}(11g_A^4 - 10g_A^2 - 1) + \frac{u^2}{10}(59g_A^4 - 50g_A^2 - 9) + \frac{1}{40}(883g_A^4 - 90g_A^2 - 73) \right. \\
& + \left. \left. \frac{3}{16u^2}(1 - 6g_A^2 - 43g_A^4) \right] \sqrt{1+u^2} \ln(u + \sqrt{1+u^2}) + \frac{3}{32u}(43g_A^4 + 6g_A^2 - 1) \right. \\
& + \frac{u}{160}(397 + 210g_A^2 - 5647g_A^4) + \frac{u^3}{5}(4 + 5g_A^2 + 31g_A^4) + \frac{u^5}{600}(119 + 710g_A^2 - 349g_A^4) \\
& \left. + \left[u^3(15g_A^4 - 6g_A^2 - 1) + \frac{u^5}{5}(11g_A^4 - 10g_A^2 - 1) \right] \ln \frac{m_\pi}{2\Lambda} \right\}, \quad (14)
\end{aligned}$$

where we have again transferred the term quadratic in the cut-off Λ to eq.(15). Obviously, terms proportional to g_A^0 , g_A^2 , g_A^4 in eq.(14) belong to the first, second, third and fourth diagram in Fig. 4, respectively. Note that the last diagram contributes both at order $\mathcal{O}(k_f^4)$ and at order $\mathcal{O}(k_f^5)$. The contribution of the Hartree-diagrams related to irreducible 2π -exchange vanishes in isospin symmetric nuclear matter for the following simple reason. After taking spin- and isospin-traces of the T-matrix, only the isoscalar central NN-amplitude $V_C(0)$ survives, and this amplitude receives no contribution from irreducible chiral 2π -exchange at leading order as shown in section 4.2 of ref.[7]. The diagrams in Fig. 4 with three medium insertions contribute only via relativistic $1/M$ -corrections at order $\mathcal{O}(k_f^6)$. Besides eq.(14), there is no further contribution at order $\mathcal{O}(k_f^5)$ from three-loop 2π -exchange diagrams. Note also that all contributions to $\bar{E}(k_f)$ remain finite in the chiral limit $m_\pi = 0$. For example, eq.(14) becomes proportional to $k_f^5[\ln(k_f/\Lambda) + const]$. As far as we can see, there are no infra-red singularities generated by the Goldstone bosons (massless pions).

Finally, we give the complete expression for the power divergences specific to cut-off regularization,

$$\bar{E}_\Lambda(k_f) = \frac{\Lambda k_f^3}{(4\pi f_\pi)^4} \left[-10g_A^4 M + (3g_A^2 + 1)(g_A^2 - 1)\Lambda \right]. \quad (15)$$

Obviously, the first term proportional to M stems from iterated 1π -exchange. The Hartree and Fock-diagrams in Fig.3 contribute to it in the ratio 4 : 1 as a result of their spin- and isospin factors. The term quadratic in the cut-off Λ , on the other hand, originates from irreducible 2π -exchange.

Eq.(15) is equivalent to the contribution of a zero-range NN-contact interaction. The cut-off scale Λ is effectively parametrizing its strength. Note that eq.(15) leads to a sizeable attraction in the hundred MeV range for physically reasonable values of the cutoff, $0.5 \text{ GeV} < \Lambda < 1.0 \text{ GeV}$. We are thus lead to the conclusion that in isospin symmetric nuclear matter 2π -exchange produces "zero-range" attraction and finite-range repulsion. It should also be noted that the dominant (real part of) iterated 1π -exchange does not have an equivalent representation as a local coordinate-space NN-potential (see section 4.3 in ref.[7]). Such a connection exists only for 1π -exchange and (with certain restrictions concerning the zero-range part) for irreducible 2π -exchange [7]. Note that $\bar{E}_\Lambda(k_f)$ in eq.(15) encodes the short-distance NN-dynamics necessary for nuclear binding. We emphasize that, for reasons of consistency, this piece (which originates from the few divergent parts of chiral 2π -exchange) should *not* be further iterated either with itself or with 1π -exchange, in contrast to what has been done with the NN-contact interaction in ref.[12].

2.5 Results

Before presenting results for the nuclear matter equation of state, we would like to exhibit the saturation mechanism. For that purpose we truncate the previous calculation of one- and two-pion exchange diagrams at order $\mathcal{O}(k_f^4)$ and we take the chiral limit, $m_\pi = 0$, (disregarding for the moment the less important Λ^2 -term in eq.(15)). In that case the complete expression for the energy per particle $\bar{E}(k_f)$ turns into the form, eq.(1), with coefficients α and β given by

$$\alpha = 10 \left(\frac{g_{\pi N}}{4\pi} \right)^4 \frac{\Lambda}{M} - \left(\frac{g_{\pi N}}{4\pi} \right)^2, \quad (16)$$

$$\beta = \frac{3}{70} \left(\frac{g_{\pi N}}{4\pi} \right)^4 (4\pi^2 + 237 - 24 \ln 2) - \frac{3}{56} = 13.55. \quad (17)$$

Note that the parameterfree expression for β gives a number quite close to $\beta = 12.22$ as extracted from the realistic equation of the state of ref.[15]. Furthermore, by adjusting the cut-off scale to $\Lambda = (0.5 \dots 0.6)M$ (which in fact lies in the physically reasonable range) α will take on its required value. Therefore, as long as the effects due to the finite pion mass and the terms at order $\mathcal{O}(k_f^5)$ do not change this picture completely, realistic nuclear binding is guaranteed by chiral pion-nucleon dynamics, together with fine-tuning of the single scale Λ representing the short-distance NN-dynamics.

Now we include all calculated terms up to order $\mathcal{O}(k_f^5)$ and we set $m_\pi = 135 \text{ MeV}$ (the neutral pion mass). We fix the (negative) binding energy to the value $\bar{E}_0 = -15.26 \text{ MeV}$ obtained in extensive and elaborate fits of nuclide masses in ref.[18]. The energy per particle $\bar{E}(k_f)$ has a minimum with this value of \bar{E}_0 at a density of $\rho_0 = 0.178 \text{ fm}^{-3}$ (corresponding to a Fermi momentum of $k_{f0} = 272.7 \text{ MeV} = 1.382 \text{ fm}^{-1}$) if the cut-off scale is fine-tuned to $\Lambda = 646.3 \text{ MeV}$. Note that a saturation density of $\rho_0 = 0.178 \text{ fm}^{-3}$ is somewhat on the large side. A slight increase of g_A by 2% would even shift ρ_0 to the center of the empirical saturation density $\rho_0 = 0.166 \text{ fm}^{-3}$ [13]. Let us also investigate how the value $\bar{E}_0 = -15.26 \text{ MeV}$ arises in the present calculation.

Its decomposition into contributions from the kinetic energy and the three classes of diagrams is $\bar{E}_0 = (23.40 + 18.24 - 68.35 + 11.45)$ MeV. On the other hand, when ordering in chiral powers $\mathcal{O}(k_f^\nu)$, ($\nu = 2, 3, 4, 5$) one finds $\bar{E}_0 = (23.75 - 154.54 + 124.61 - 9.08)$ MeV. The individual entries follow closely the pattern prescribed by the parametrization eq.(1) with a balance between large third and fourth order terms. If the behavior of the last two entries is representative the chiral expansion of \bar{E}_0 appears to converge.

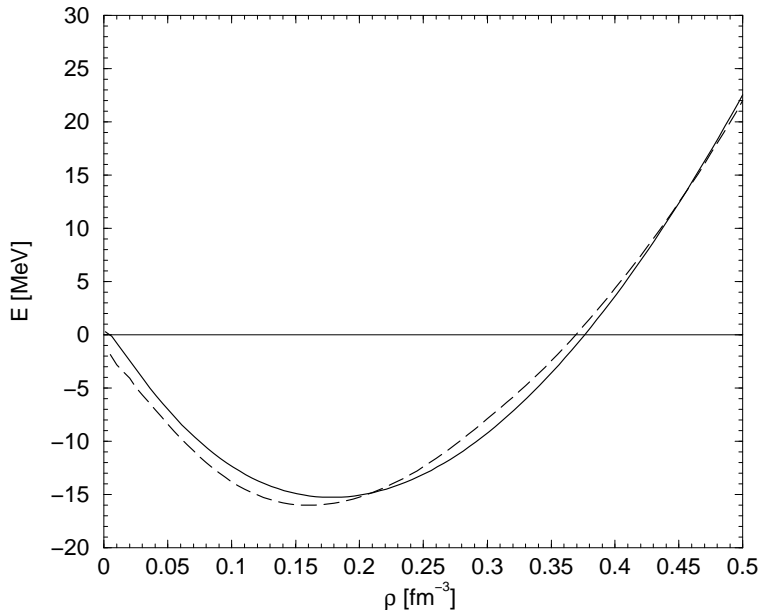


Fig. 5: Energy per particle of isospin symmetric nuclear matter derived from chiral one- and two-pion exchange (solid line). The value of the cut-off scale is $\Lambda = 646$ MeV. The dashed line corresponds to the result of ref.[15].

In Fig. 5 we show the resulting nuclear equation of state for densities up to $\rho = 0.5 \text{ fm}^{-3}$ (i.e. about $3\rho_0$). The nuclear compressibility K related to the curvature of the saturation curve at its minimum comes out as $K = 255$ MeV, in very good agreement with the nowadays accepted empirical value $K = (250 \pm 25)$ MeV [13, 14] (for the definition of K , see eq.(2)).

Fig. 6 shows by the solid line the dependence of the saturation point (ρ_0, \bar{E}_0) on the cut-off Λ which has been varied in the range $0.6 \text{ GeV} < \Lambda < 0.7 \text{ GeV}$. The inserted rectangle corresponds to the empirical saturation “point” $\bar{E}_0 = (-16 \pm 1)$ MeV and $k_{f0} = (1.35 \pm 0.05) \text{ fm}^{-1}$ quoted in ref.[4]. The variation of the saturation point (ρ_0, \bar{E}_0) in Fig. 6 is somewhat reminiscent of the familiar Coester-line; of course, the physics behind it is quite different here. It is gratifying that our line meets the empirical saturation “point”. The dashed line in Fig. 6, which gives the calculated saturation point in the chiral limit, $m_\pi = 0$ (keeping g_A, M, f_π fixed), is also interesting. It suggests that in QCD explicit chiral symmetry breaking is not a crucial condition for nuclear binding. Note however that for fixed Λ , taking the chiral limit $m_\pi = 0$, increases the binding energy \bar{E}_0 as well as the equilibrium density ρ_0 considerably.

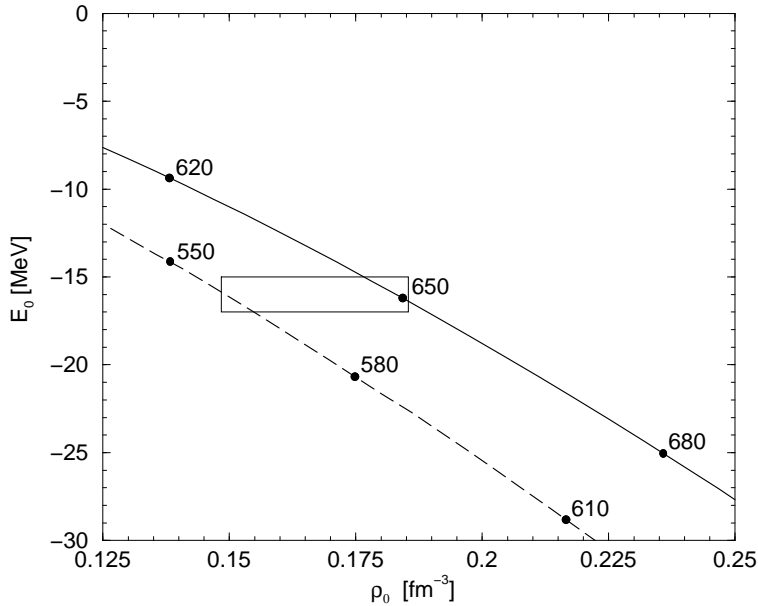


Fig. 6: The nuclear matter saturation point (ρ_0, \bar{E}_0) at finite pion mass (solid line) and in the chiral limit (dashed line) as a function of the cut-off scale Λ (points in MeV). The inserted rectangle corresponds to the empirical saturation “point”.

3 Asymmetry energy

The properties of isospin symmetric matter can be well reproduced in our framework with just one single adjustable cut-off scale Λ . In order to test the isospin dependence of the underlying pion-exchange dynamics which causes saturation, we now investigate the asymmetry energy. In isospin asymmetric matter the Fermi seas of protons and neutrons are filled unequally. With the help of the projection operators $(1 \pm \tau_3)/2$ such an isospin-asymmetric situation is realized by the simple substitution,

$$\theta(k_f - |\vec{p}|) \rightarrow \frac{1 + \tau_3}{2} \theta(k_p - |\vec{p}|) + \frac{1 - \tau_3}{2} \theta(k_n - |\vec{p}|), \quad (18)$$

in the in-medium nucleon propagator eq.(3). Here k_p and k_n denote the (different) Fermi momenta of protons and neutrons. Choosing $k_{p,n} = k_f(1 \mp \delta)^{1/3}$ (with δ a small parameter) the nucleon density $\rho = \rho_p + \rho_n = (k_p^3 + k_n^3)/3\pi^2 = 2k_f^3/3\pi^2$ stays constant. The expansion of the energy per particle of isospin asymmetric nuclear matter,

$$\bar{E}_{as}(k_p, k_n) = \bar{E}(k_f) + \delta^2 A(k_f) + \dots, \quad (19)$$

around the symmetry line ($k_p = k_n$ or $\delta = 0$) defines the asymmetry energy $A(k_f)$. Note that the parameter δ is equal to $(\rho_n - \rho_p)/(\rho_n + \rho_p)$ or $(N - Z)/(N + Z)$. Differences in comparison with the diagrammatic calculation in section 2 occur only with respect to isospin factors and the radii of the Fermi spheres, $k_p = k_f(1 - \delta)^{1/3}$ or $k_n = k_f(1 + \delta)^{1/3}$. Following the scheme in section 2, we summarize the individual contributions to the asymmetry energy $A(k_f)$ without going into further technical details.

i) Kinetic energy of a relativistic Fermi gas:

$$A_k(k_f) = \frac{k_f^2}{6M} - \frac{k_f^4}{12M^3}. \quad (20)$$

The next term in this series, $k_f^6/16M^5$, is negligibly small.

ii) 1π -exchange Fock-diagram including the relativistic $1/M^2$ -correction:

$$A_1(k_f) = \frac{g_A^2 m_\pi^3}{(4\pi f_\pi)^2} \left\{ \left(\frac{u}{3} + \frac{1}{8u} \right) \ln(1+4u^2) - \frac{u}{2} - \frac{u^3}{3} + \frac{m_\pi^2}{M^2} \left[u^3 - \frac{u^2}{2} \arctan 2u - \frac{u^3}{3} \ln(1+4u^2) \right] \right\}, \quad (21)$$

with the abbreviation $u = k_f/m_\pi$.

iii) Hartree-diagram in Fig. 3 with two medium insertions:

$$A_2(k_f) = \frac{g_A^4 M m_\pi^4}{(8\pi)^3 f_\pi^4} \left\{ \left(\frac{25}{3}u + \frac{7}{6u} \right) \ln(1+4u^2) - \frac{14}{3}u - 16u^2 \arctan 2u \right\}. \quad (22)$$

iv) Fock-diagram in Fig. 3 with two medium insertions:

$$A_3(k_f) = \frac{g_A^4 M m_\pi^4}{(4\pi)^3 f_\pi^4} \left\{ -\frac{5}{6}u^3 + \int_0^u dx \frac{3x^2 - 4u^2}{6u(1+2x^2)} \left[(1+8x^2+8x^4) \arctan x - (1+4x^2) \arctan 2x \right] \right\}. \quad (23)$$

v) Hartree-diagram in Fig. 3 with three medium insertions:

$$\begin{aligned} A_4(k_f) &= \frac{g_A^4 M m_\pi^4}{(4\pi f_\pi)^4 u^3} \int_0^u dx x^2 \int_{-1}^1 dy \left\{ \left[\frac{uxy(26u^2 - 30x^2y^2)}{3(u^2 - x^2y^2)} + (3u^2 - 5x^2y^2)H \right] \right. \\ &\times \left[\frac{2s^2 + s^4}{1+s^2} - 2 \ln(1+s^2) \right] - \frac{4u^2 H s^6}{3(1+s^2)^2} + \left[2uxy + (u^2 - x^2y^2)H \right] \\ &\times \left. \left[(5+s^2)(3s^2 - 8ss' + 8s'^2) + 8s(1+s^2)(s'' - 5s' + 3s) \right] \frac{s^4}{3(1+s^2)^3} \right\}. \quad (24) \end{aligned}$$

The auxiliary functions H and s have been defined in eq.(10) and s' and s'' denote partial derivatives,

$$s' = u \frac{\partial s}{\partial u}, \quad s'' = u^2 \frac{\partial^2 s}{\partial u^2}. \quad (25)$$

vi) Fock-diagram in Fig. 3 with three medium insertions:

$$\begin{aligned} A_5(k_f) &= \frac{g_A^4 M m_\pi^4}{(4\pi f_\pi)^4 u^3} \int_0^u dx \left\{ \frac{G}{24} (3G_{20} - 2G_{11} + 3G_{02} - 8G_{01} - 3G) + \frac{G_{10} + G_{01}}{24} (3G_{10} - 5G_{01}) \right. \\ &+ \frac{x^2}{6} \int_{-1}^1 dy \int_{-1}^1 dz \frac{yz \theta(y^2 + z^2 - 1)}{|yz| \sqrt{y^2 + z^2 - 1}} \left[\frac{2s^3 t^4 (8s' - 3s)}{(1+s^2)(1+t^2)} \right. \\ &\left. \left. + \left[(3+s^2)(8ss' - 3s^2 - 8s'^2) + 4s(1+s^2)(6s' - 3s - 2s'') \right] \frac{s^2 [t^2 - \ln(1+t^2)]}{(1+s^2)^2} \right] \right\}. \quad (26) \end{aligned}$$

The auxiliary functions G and t have been defined in eqs.(12,13) and we have introduced the following double-index notation for partial derivatives of the function G ,

$$G_{ij} := x^i u^j \frac{\partial^{i+j} G}{\partial x^i \partial u^j}, \quad 1 \leq i+j \leq 2. \quad (27)$$

vii) Irreducible 2π -exchange Hartree- and Fock-diagrams in Fig. 4:

$$A_6(k_f) = \frac{m_\pi^5}{(4\pi f_\pi)^4} \left\{ \left[\frac{1}{12u} (1 - 2g_A^2 - 23g_A^4) + \frac{u}{3} (1 + 2g_A^2 - 7g_A^4) \right] \ln^2(u + \sqrt{1+u^2}) \right.$$

$$\begin{aligned}
& + \left[\frac{1}{6}(23g_A^4 + 2g_A^2 - 1) + u^2 \left(\frac{1}{3} + 2g_A^2 - 5g_A^4 \right) - \frac{16}{3}g_A^4 u^4 \right] \sqrt{1+u^2} \ln(u + \sqrt{1+u^2}) \\
& + \frac{u}{12}(1 - 2g_A^2 - 23g_A^4) + u^3 \left(\frac{1}{4} + \frac{11}{2}g_A^2 - \frac{245}{12}g_A^4 \right) - \frac{u^5}{27}(1 + 10g_A^2 + g_A^4) \\
& + u^3 \left[\frac{5}{3} + 10g_A^2 - 25g_A^4 - \frac{16}{3}g_A^4 u^2 \right] \ln \frac{m_\pi}{2\Lambda} \}. \tag{28}
\end{aligned}$$

The Hartree-diagrams (not shown in Fig. 4) give a contribution to the asymmetry energy $A(k_f)$ through the isovector central NN-amplitude $W_C(0)$ (see section 4.2 in ref.[7]). In terms of this amplitude the contribution of the irreducible 2π -exchange Hartree-diagrams reads $A(k_f) = -\rho W_C(0)/2$.

viii) Power divergences specific for cut-off regularization:

$$A_\Lambda(k_f) = \frac{\Lambda k_f^3}{3(4\pi f_\pi)^4} \left[26g_A^4 M + 5(3g_A^2 + 1)(1 - g_A^2)\Lambda \right]. \tag{29}$$

Again, this expression collects the contributions from iterated 1π -exchange and irreducible 2π -exchange. In comparison to $\bar{E}_\Lambda(k_f)$ given in eq.(15) the term, eq.(29), has changed sign. The isospin-structure of the underlying 2π -exchange interaction shows up in the linear and quadratic term in Λ through relative factors $-13/15$ and $-5/3$, respectively.

As a side remark we note that in the chiral limit, $m_\pi = 0$, the order $\mathcal{O}(k_f^4)$ contributions to the asymmetry energy $A(k_f)$ (see eqs.(22,23,24,26)) can be evaluated in closed form with the result,

$$A(k_f)|_{m_\pi=0} = - \left(\frac{g_A k_f}{4\pi f_\pi} \right)^4 \frac{M}{135} (44\pi^2 + 987 + 216 \ln 2). \tag{30}$$

For the numerical evaluation of the asymmetry energy we use the same parameter input as in section 2.5, in particular a cut-off scale of $\Lambda = 646.3$ MeV. The value of the asymmetry energy $A(k_f)$ at our saturation point $k_{f0} = 272.7$ MeV comes out as $A_0 = A(k_{f0}) = 33.8$ MeV. This is in very good agreement with the empirical value of $A_0 = 33.2$ MeV obtained in ref.[18] from extensive and elaborate fits to nuclide masses. Let us again investigate how the value $A_0 = 33.8$ MeV arises in the present calculation. Its decomposition into contributions from the kinetic energy and the three classes of diagrams is $A_0 = (12.7 - 5.3 + 40.7 - 14.3)$ MeV. On the other hand, when ordering in chiral powers $\mathcal{O}(k_f^\nu)$, ($\nu = 2, 3, 4, 5$) one finds $A_0 = (13.2 + 129.9 - 127.4 + 18.1)$ MeV. Here, one observes an almost complete cancelation of large third and fourth order terms. Again, if the behavior of the last two entries is representative, the chiral expansion of the asymmetry energy A_0 should converge.

In Fig. 7 we show by the solid line the dependence of the asymmetry energy $A(k_f)$ on the density $\rho = 2k_f^3/3\pi^2$. One observes that $A(k_f)$ reaches its maximum close to the saturation density ρ_0 . We obtain therefore a small value of the (empirically not well determined) slope parameter $L = k_{f0}[\partial A(k_f)/\partial k_f]_0 = 14.7$ MeV (see also ref.[13]). Furthermore, we extract an asymmetry compressibility of $K_{as} = k_{f0}^2[\partial^2 A(k_f)/\partial k_f^2]_0 - 2L = -359$ MeV. Such large and negative values of K_{as} are also found in some other calculations (see table 4 in ref.[13]). For comparison we show in Fig. 7 also the result for the asymmetry energy $A(k_f)$ obtained in the Brückner-Hartree-Fock calculation of ref.[19]. The downward bending of our asymmetry energy $A(k_f)$ at densities $\rho > 0.2 \text{ fm}^{-3}$ presumably indicates the limits of validity of the present chiral perturbation theory calculation of nuclear matter.

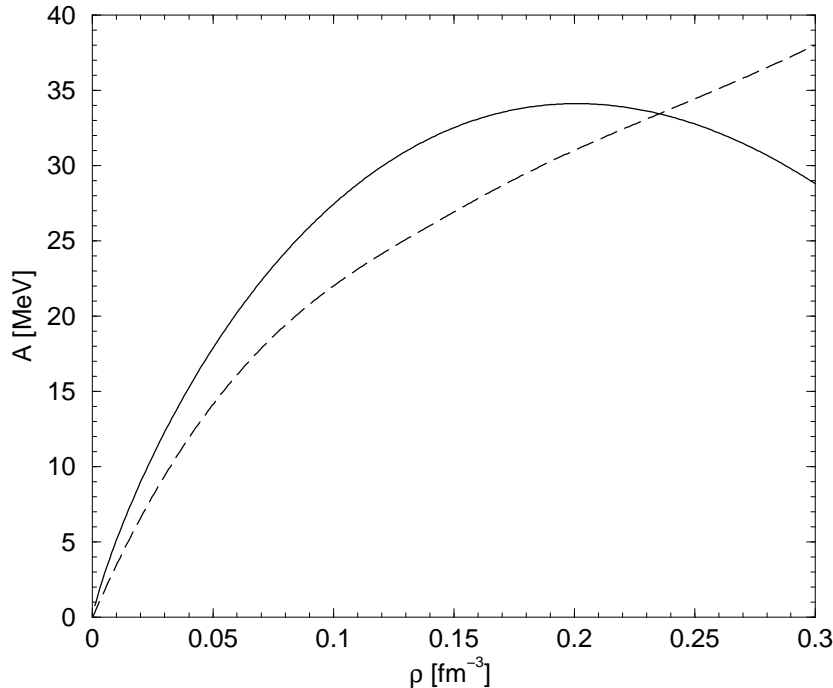


Fig. 7: The density dependence of the asymmetry energy $A(k_f)$ (solid line). The cut-off is $\Lambda = 646$ MeV. The dashed line gives the result of ref.[19].

The simultaneous correct description of several nuclear matter properties (saturation point, compressibility, asymmetry energy) with only one adjustable scale parameter, the cut-off Λ , is indeed highly non-trivial. This strongly indicates that nuclear binding and saturation through the combination of chiral one- and two-pion exchange and short-distance dynamics encoded in a single high momentum scale Λ is a realistic scenario (at low densities $\rho \leq 0.2 \text{ fm}^{-3}$). Our treatment of the zero-range components of the effective NN-interaction in terms of a cut-off Λ seems to work surprisingly well and it resembles effects of correlation functions in sophisticated many-body calculations.

4 Neutron matter

The extreme of asymmetric nuclear matter is pure neutron matter. All existing realistic calculations [15, 20, 21, 22] agree that pure neutron matter is unbound. Its energy per particle monotonically rises with the neutron density.

In order to arrive at the energy per particle, $\bar{E}_n(k_n)$, of neutron matter in our diagrammatic framework it is sufficient to make the substitution

$$\theta(k_f - |\vec{p}|) \rightarrow \frac{1 - \tau_3}{2} \theta(k_n - |\vec{p}|), \quad (31)$$

in the in-medium nucleon propagator eq.(3). Here k_n denotes the Fermi momentum of the neutrons related to the neutron density by $\rho_n = k_n^3/3\pi^2$. As a consequence of the substitution eq.(31) only the isospin factors of individual diagrams change and all Fermi spheres have the radius k_n . We follow the scheme in section 3 and enumerate the individual contributions to the energy per particle, $\bar{E}_n(k_n)$, of neutron matter.

i) Kinetic energy of a relativistic Fermi gas:

$$\bar{E}_{n,k}(k_n) = \frac{3k_n^2}{10M} - \frac{3k_n^4}{56M^3}. \quad (32)$$

ii) 1π -exchange Fock-diagram including the relativistic $1/M^2$ -correction:

$$\begin{aligned} \bar{E}_{n,1}(k_n) = & \frac{g_A^2 m_\pi^3}{(4\pi f_\pi)^2} \left\{ \frac{u^3}{3} + \frac{1}{8u} - \frac{3u}{4} + \arctan 2u - \left(\frac{3}{8u} + \frac{1}{32u^3} \right) \ln(1 + 4u^2) \right. \\ & \left. + \frac{m_\pi^2}{40M^2} \left[\frac{40}{3}u^3 - 8u^5 + 9u + \frac{1}{2u} - (12u^2 + 5) \arctan 2u - \frac{1}{8u^3} \ln(1 + 4u^2) \right] \right\} \quad (33) \end{aligned}$$

We emphasize that in this section the meaning of u changes to $u = k_n/m_\pi$.

iii) Hartree-diagram in Fig. 3 with two medium insertions:

$$\bar{E}_{n,2}(k_n) = \frac{g_A^4 M m_\pi^4}{10(8\pi)^3 f_\pi^4} \left\{ \frac{9}{2u} - 59u + (60 + 32u^2) \arctan 2u - \left(\frac{9}{8u^3} + \frac{35}{2u} \right) \ln(1 + 4u^2) \right\}. \quad (34)$$

iv) Fock-diagram in Fig. 3 with two medium insertions:

$$\bar{E}_{n,3}(k_n) = \frac{g_A^4 M m_\pi^4}{(4\pi)^3 f_\pi^4} \left\{ -\frac{u^3}{6} + \int_0^u dx \frac{x(u-x)^2(2u+x)}{2u^3(1+2x^2)} \left[(1+4x^2) \arctan 2x - (1+8x^2+8x^4) \arctan x \right] \right\}. \quad (35)$$

v) Hartree-diagram in Fig. 3 with three medium insertions:

$$\bar{E}_{n,4}(k_n) = \frac{3g_A^4 M m_\pi^4}{(4\pi f_\pi)^4 u^3} \int_0^u dx x^2 \int_{-1}^1 dy \left[2uxy + (u^2 - x^2 y^2) H \right] \left\{ \frac{2s^2 + s^4}{2(1+s^2)} - \ln(1+s^2) \right\}. \quad (36)$$

vi) Fock-diagram in Fig. 3 with three medium insertions:

$$\bar{E}_{n,5}(k_n) = \frac{3g_A^4 M m_\pi^4}{(4\pi f_\pi)^4 u^3} \int_0^u dx \left\{ -\frac{G^2}{8} + \frac{x^2}{4} \int_{-1}^1 dy \int_{-1}^1 dz \frac{yz \theta(y^2 + z^2 - 1)}{|yz| \sqrt{y^2 + z^2 - 1}} \left[s^2 - \ln(1+s^2) \right] \left[t^2 - \ln(1+t^2) \right] \right\}. \quad (37)$$

vii) Irreducible 2π -exchange Hartree- and Fock-diagrams in Fig. 4:

$$\begin{aligned} \bar{E}_{n,6}(k_n) = & \frac{m_\pi^5}{(4\pi f_\pi)^4} \left\{ \left[\frac{1}{32u^3} (83g_A^4 + 6g_A^2 - 1) + \frac{1}{4u} (47g_A^4 + 2g_A^2 - 1) \right] \ln^2(u + \sqrt{1+u^2}) \right. \\ & + \left[\frac{u^2}{30} (3g_A^4 - 50g_A^2 - 9) - \frac{u^4}{15} (13g_A^4 + 10g_A^2 + 1) + \frac{1}{120} (1691g_A^4 - 90g_A^2 - 73) \right. \\ & \left. + \frac{1}{16u^2} (1 - 6g_A^2 - 83g_A^4) \right] \sqrt{1+u^2} \ln(u + \sqrt{1+u^2}) + \frac{1}{32u} (83g_A^4 + 6g_A^2 - 1) \\ & + \frac{u}{480} (397 + 210g_A^2 - 11159g_A^4) + \frac{u^5}{1800} (119 + 710g_A^2 + 107g_A^4) \\ & \left. + \frac{u^3}{15} (9 + 55g_A^2 - 108g_A^4) + \left[u^3 \left(\frac{1}{3} + 2g_A^2 - 5g_A^4 \right) - \frac{u^5}{15} (13g_A^4 + 10g_A^2 + 1) \right] \ln \frac{m_\pi}{2\Lambda} \right\}. \quad (38) \end{aligned}$$

This expression includes the contributions from Hartree diagrams (not shown in Fig. 4) via the isovector central NN-amplitude $W_C(0)$ (see section 4.2 in ref.[7]). In terms of this amplitude the contribution of the irreducible 2π -exchange Hartree-diagrams is, $\bar{E}_n(k_n) = -\rho_n W_C(0)/2$.

viii) Power divergences specific for cut-off regularization:

$$\bar{E}_{n,\Lambda}(k_n) = -\frac{\Lambda k_n^3}{3(4\pi f_\pi)^4} \left[2g_A^4 M + (3g_A^2 + 1)(g_A^2 - 1)\Lambda \right]. \quad (39)$$

Note that compared to eq.(15) the attraction in neutron matter gets strongly reduced. This welcome feature has its origin in the isospin dependence of the 2π -exchange.

In the chiral limit, $m_\pi = 0$, and truncated at order $\mathcal{O}(k_f^4)$ the equation of state of neutron matter $\bar{E}_n(k_n)$ turns also into the form eq.(1) with the coefficient $\beta_n = (g_{\pi N}/4\pi)^4 (27 - 4\pi^2 - 24 \ln 2)/70 - (3/56) = -0.562$. The other coefficient α_n can be easily read off from eqs.(33,39).

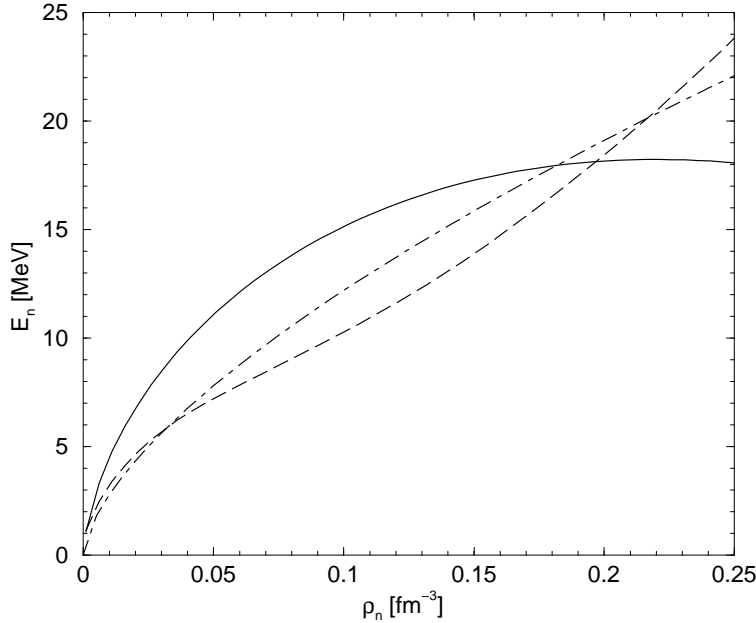


Fig. 8: The equation of state of pure neutron matter $\bar{E}_n(k_n)$. The dashed line corresponds to the many-body calculation of ref.[15]. The dashed-dotted line represents eq.(40) with a neutron-neutron scattering length of $a_{nn} = 18.7$ fm. The full line gives the result of chiral one- and two-pion exchange with a cutoff of $\Lambda = 646$ MeV.

If we use the same parameter input as in section 2.5, the resulting equation of state of neutron matter, $\bar{E}_n(k_n)$, comes out as the solid line in Fig. 8. The convex shape of the curve is generic and does not change much with the cut-off Λ . It demonstrates the limitations of our present perturbative approach. The dashed line in Fig. 8 corresponds to the many-body calculation of the Urbana group [15]. This curve should be considered as a representative of the host of existing neutron matter calculations [20, 21, 22] which scatter around it. One observes a rough agreement up to neutron densities of about $\rho_n = 0.25$ fm $^{-3}$. At higher densities our neutron equation of state starts to become unrealistic because of its downward bending ($\beta_n < 0$). This feature is inherited from the asymmetry energy $A(k_f)$ (see Fig. 7). Note however that our prediction for the neutron matter equation of state is still much better than the one of the $\sigma\omega$ -mean field model [23] (for low neutron densities $\rho_n < 0.25$ fm $^{-3}$).

The complete resummation of in-medium multi-loop diagrams for a system with an unnaturally large scattering length has been achieved in the limit of large space-time dimensions D in ref.[11]. Neglecting the $1/D$ -corrections (approximately less than 20%) the result of Steele [11] applied to neutron matter reads,

$$\bar{E}_n(k_n) = \frac{k_n^2}{M} \left[\frac{3}{10} - \frac{a_{nn} k_n}{3\pi + 6a_{nn} k_n} \right], \quad (40)$$

with a_{nn} the neutron-neutron scattering length. A recent measurement [24] has found the precise value $a_{nn} = (18.7 \pm 0.6)$ fm. (We use that sign-convention in which a positive scattering length corresponds to attraction.) The density dependence of eq.(40) is shown by the dashed-dotted line in Fig. 8. The agreement with the many-body calculation of ref.[15] is somewhat better.⁴ Interestingly, the dashed-dotted line does almost not change if the nn -scattering length is sent to infinity, $a_{nn} = \infty$, where $\bar{E}_n(k_n) = 2k_n^2/15M$.

Concerning our neutron matter equation of state (solid line in Fig. 8) one should not forget that it has no free parameters (assuming that the high momentum scale Λ is the same as in isospin symmetric nuclear matter). The fair agreement with the other two curves (for $\rho_n \leq 0.25 \text{ fm}^{-3}$) is therefore quite surprising. The mere fact the neutron matter is predicted to be unbound is already non-trivial.

5 Summary and Outlook

The present work can be summarized as follows: We have used chiral perturbation theory to calculate the nuclear matter equation of state systematically up to three-loops. The contributions to the energy per particle $\bar{E}(k_f)$ from one- and two-pion exchange diagrams are ordered in powers of the Fermi momentum k_f (modulo functions of k_f/m_π). We have evaluated all contributions up-to-and-including order $\mathcal{O}(k_f^5)$.

A momentum cut-off scale Λ has been used to regularize the few divergent parts associated with chiral 2π -exchange. The terms linear and quadratic in Λ effectively parametrize an equivalent zero-range NN-contact interaction which is strongly attractive in isospin symmetric nuclear matter. Its isospin dependence is revealed (and tested) in the asymmetry energy $A(k_f)$.

The saturation mechanism behind the chiral 2π -exchange is easy to understand (in the chiral limit $m_\pi = 0$). An attractive $\alpha k_f^3/M^2$ term plus a repulsive $\beta k_f^4/M^3$ term, with proper coefficients α and β , lead automatically to a realistic nuclear matter equation of state.

Without inclusion of any further short-range terms, and adjusting the cut-off scale to the physically sensible value $\Lambda \simeq 0.65$ GeV, the empirical saturation point ($\rho_0 \simeq 0.17 \text{ fm}^{-3}$, $\bar{E}_0 \simeq -15$ MeV) and the nuclear compressibility $K \simeq 250$ MeV are well reproduced. Decomposing the binding energy \bar{E}_0 into chiral orders one recovers the pattern of the realistic (α, β) -parametrization. We note in passing that the present calculation gives a single particle potential for a nucleon at rest in equilibrium nuclear matter which amount to $U(0, k_{f0}) \simeq -53$ MeV [25].

In the same framework and using the same parameters the density dependent asymmetry energy $A(k_f)$ has been calculated. The prediction for the asymmetry energy at the saturation point $A_0 \simeq 34$ MeV is in very good agreement with the empirical value. This is achieved again with just one cut-off Λ instead of introducing additional contact terms: apparently, one single cut-off scale is enough to represent the relevant short-distance dynamics. The downward bending of $A(k_f)$ at $\rho > 0.2 \text{ fm}^{-3}$ presumably indicates the limits of validity of the present chiral perturbation theory calculation of nuclear matter.

The equation of state of pure neutron matter as predicted in this framework is also in rough agreement with sophisticated many-body calculations and a resummation result of effective field theory for neutron densities ρ_n less than 0.25 fm^{-3} . The mere fact that neutron matter comes out unbound is non-trivial.

The present approach to the nuclear matter problem is quite different from most other commonly used ones. We do neither start from a (so-called) realistic NN-potential which fits the deuteron properties and the NN-phase shifts, nor do we employ relativistic mean field methods.

⁴We have assumed here that eq.(40) can be extrapolated to Fermi momenta as large as $k_n = 385$ MeV.

Nevertheless, we find realistic nuclear binding, including its isospin dependence, already at the level of the three-loop approximation of in-medium chiral perturbation theory.

Questions remain, of course, whether the good results obtained so far survive in higher orders. Relativistic $1/M$ -corrections seem to present no problem since they are in general small (as long as the densities are not too high). Two-pion exchange with virtual $\Delta(1232)$ -resonance excitation produces essentially all the medium-range scalar-isoscalar attraction which is needed for the description of the peripheral NN-scattering [8]. In the nuclear matter calculation the short-range contributions from 2π -exchange with $\Delta(1232)$ -excitation as well as additional Pauli-blocking effects (related to diagrams with three medium insertions) come also into play. At the present stage, such effects are possibly hidden in the cut-off scale Λ ; at a higher level of "resolution", they can and have to be studied explicitly in the framework of chiral effective field theory. Work along this line is in progress.

Acknowledgement

We thank P. Ring for useful discussions.

References

- [1] A. Akmal, V.R. Pandharipande, D.G. Ravenhall, *Phys. Rev.* **C58** (1998) 1804; and refs. therein.
- [2] B.D. Serot and J.D. Walecka, *Adv. Nucl. Phys.* **16** (1986) 1; and refs. therein.
- [3] P. Ring, *Prog. Part. Nucl. Phys.* **37** (1996) 193; and refs. therein.
- [4] R. Brockmann and R. Machleidt, *Phys. Rev.* **C42** (1990) 1965; and refs. therein.
- [5] D.B. Kaplan, M.J. Savage and M.B. Wise, *Nucl. Phys.* **B534** (1998) 329.
- [6] E. Epelbaum, W. Glöckle and Ulf-G. Meißner, *Nucl. Phys.* **A671** (2000) 295; and refs. therein.
- [7] N. Kaiser, R. Brockmann and W. Weise, *Nucl. Phys.* **A625** (1997) 758.
- [8] N. Kaiser, S. Gerstendörfer and W. Weise, *Nucl. Phys.* **A637** (1998) 395.
- [9] R.J. Furnstahl, J.V. Steele and N. Tifessa, *Nucl. Phys.* **A671** (2000) 396.
- [10] H.W. Hammer and R.J. Furnstahl, *Nucl. Phys.* **A678** (2000) 277.
- [11] J.V. Steele, "Effective field theory power counting at finite density", nucl-th/0010066.
- [12] M. Lutz, B. Friman and C. Appel, *Phys. Lett.* **B474** (2000) 7.
- [13] J.P. Blaizot, *Physics Reports* **64** (1980) 171.
- [14] D. Vretenar et al., *Nucl. Phys.* **A621** (1997) 853; P. Ring, private communications.
- [15] B. Friedman and V.R. Pandharipande, *Nucl. Phys.* **A361** (1981) 502.
- [16] M.M. Pavan et al., *Physica Scripta* **T87** (2000) 65.
- [17] L. Onsager, L. Mittag and M.J. Stephen, *Ann. der Physik (Leipzig)* **18** (1966) 71.
- [18] P.A. Seeger and W.M. Howard, *Nucl. Phys.* **A238** (1975) 491.
- [19] W. Zuo, I. Bombaci and U. Lombardo, *Phys. Rev.* **C60** (1999) 024605.
- [20] R.B. Wiringa, V. Fiks and A. Fabrocini, *Phys. Rev.* **C38** (1988) 1010.
- [21] N.K. Glendenning, *Nucl. Phys.* **A493** (1989) 521.
- [22] G.Q. Li, R. Machleidt and R. Brockmann, *Phys. Rev.* **C45** (1992) 2782.
- [23] S.A. Chin and J.D. Walecka, *Phys. Lett.* **B52** (1974) 24.
- [24] D.E. Gonzalez Trotter et al., *Phys. Rev. Lett.* **83** (1999) 3788.
- [25] N. Kaiser, S. Fritsch and W. Weise, in preparation.